RESEARCH PAPER

Thyroid Nodule Image Joint Segmentation and Classification Based on Deep Learning

[1]Firas Husham Al-Mukhtar, [*]Dilshad Salih Ismael, [2]Raghad Zuhair Yousif, [3]Salih Omer Haji, [4]BazhdarNooraddin Mohammed

[2-4,*]Department of Physics, College of Science, Salahaddin University-Erbil, Kurdistan Region, Iraq

[1,2] Department of Computer Science and Information Technology, Catholic University in Erbil, Kurdistan Region, Iraq

A B S T R A C T:

A thyroid nodule is a thyroid gland condition that must be diagnosed and treated as soon as possible to mitigate the threat of death in a possible patient. This research proposed a joint segmentation and classification system to detect and identify thyroid nodules in ultrasound images automatically. The proposed scheme as it is envisioned has consist of two stages: in the first stage thyroid image features were calculated via a concatenation of features vector (to enhance the diversity of image features)generated by deep learning-based VGG-19 model in the first place and the second place by deriving handmade features from VGG-SegNet image segmentation model followed by computing a Fuzzy Grey Level Co-Occurrence Matrix (FGLCM) for each segmented image, which has the effect of eliminating directional difference by multi-angle fusing the grey level co-occurrence matrix (GLCM) and calculation of the membership of each pixel to the texture unit after applying the fuzzy c-means algorithm to the grey level co-occurrence matrix. The second stage then involves thyroid image classification based on four types of machine learning techniques namely (Naïve Bayes NB, Decision Tree DT, K-Nearest Neighbor KNN, and SVM-RBF Support Vector Machine based Radial Basis Function). The proposed model has been evaluated based on Thyroid Digital Image Database (TDID), which is a public dataset for thyroid nodule segmentation created by Universidad Nacional de Colombia. The experimental results revealed that the SVM-RBF classifier has achieved a validation accuracy of 99.25% with concatenated features vector.

1. INTRODUCTION:

The thyroid is one of the body's endocrine glands, which secrete hormones to control other hormones. The butterfly-shaped thyroid gland, which sits low in the front of the neck and is encircled by the larynx and trachea, is important in the body (Rehman et al., 2021). Thyroid nodule malignancy is a medical problem characterized by benign or malignant irregular cell development (Acharya et al., 2016). Nodules form when cells in the thyroid gland multiply or lesions develop; they can be isolated, clustered, or fused. Only around 0.1% to 0.2% of thyroid nodules are malignant (Koundal et al., 2018).

Thyroid nodule segmentation is a critical step in computer-assisted thyroid nodule identification using ultrasound images. However, due to low contrast, excessive noise, variable appearance, and complicated thyroid nodule structure segmenting lesions from ultrasound images remain difficult. As a result, accurate nodule diagnosis requires substantial clinical knowledge and competence (Ajilisa et al., 2022, Haji and Yousif, 2019).

Over the last three decades, thyroid cancer has been one of the fastest-increasing diseases in the United States (Cheng et al., 2010). The majority of this rise in identification appears to be the consequence of greater thyroid ultrasonography usage, which can reveal previously undiscovered thyroid nodules. In

* **Corresponding Author:**
Dilshad Salih Ismael
E-mail: dilshad.ismael@su.edu.krd

thyroid radiology, ultrasound imaging is the most extensively used tool for assessing thyroid nodules (Nguyen et al., 2020). An accurate thyroid nodule diagnosis is the most important factor in a successful surgical outcome. CAD tools, in addition to traditional approaches, have become more common in clinical diagnostics (Zhang et al., 2019). The objective of digitalizing illness detection is to enhance diagnosis accuracy while lowering patient expenditures and length of stay. To improve the thyroid ultrasound CAD system, automated Machine Learning (ML) techniques were used. Deep Learning (DL), a subdomain of Machine Learning (ML), has grown rapidly in diagnostic imaging analysis and is frequently acknowledged as a viable option for analyzing ultrasound images (Sharifi et al., 2021).

Previous research has given numerous strategies for finding nodules in ultrasonic images. Prochazka et al. proposed a CAD system for detecting thyroid nodules by analyzing direction-independent characteristics in ultrasound images with a histogram and a segmentation-based fractal morphological analysis technique (Prochazka et al., 2019). To distinguish between benign and malignant thyroid nodules, SVM and a random forest classifier were used. To achieve a more accurate diagnosis, the authors used segmentation techniques to improve nodule categorization.

Ajilisa et al report that U-Net can properly define nodules without human involvement and that all segmentation algorithms rely on residual learning (Ajilisa, et al., 2022). This approach can help the radiologist make decisions with less input from the operators.

Yang and colleagues introduced a deep-learning architecture for accurately predicting benign and malignant thyroid nodules (Yang et al., 2022). They utilize a ResNet18 model that has been pre-trained on ImageNet to classify thyroid lesions. Using deep learning and ultrasound images, this model proved the possibility of assessing benign and malignant thyroid nodules. Various approaches for detecting thyroid nodules have been provided in previous research. Kataoka et al described feature assessment on various deep-learning networks for object recognition and detection. They compared the VGG-Net architecture to the Alex Net design. They also used Principal Component Analysis (PCA) to tune features by concatenating select layers from both

architectures (Kataoka et al., 2015). Another study on identifying and categorizing four distinct types of thyroid nodules was published by Vasile et al in which a clustering algorithm that combined two deep learning models had been proposed with an overall accuracy of 97.35%, the ensemble CNN-VGG approach outperformed the 5-CNN and VGG-19 models (Vasile et al., 2021). Deep learning models, such as U-Net have recently demonstrated promising results in medical image segmentation tasks, and have emerged as the most active study focuses in this field (Ying et al., 2018). When compared to the previously described conventional image segmentation techniques, the deep learning approach dramatically enhanced segmentation accuracy and automation.

Wang Xin and Xu Wenjie proposed a nodule segmentation approach that uses spatially limited fuzzy C-means clustering and a local fitting RSF model (Wang and Xu 2016), however, the clustering parameters in this method must be selected manually, which increased the efforts of the operation. Ma J et al. used a deep convolutional neural network to segment ultrasound images of thyroid nodules, trained the neural network with image blocks, and achieved better results than traditional semi-automatic segmentation methods (Ma et al., 2017), demonstrating the benefits of convolutional neural networks in thyroid nodule ultrasound segmentation. Ying et al. proposed an alternative method for segmenting thyroid nodules to the usual end-to-end segmentation approach (Ying et al., 2018). The U-net network was utilized to extract the area of interest (ROI) of thyroid nodules, followed by rough manual labeling, and lastly, the VGG19 network was used to carefully segment thyroid nodules.

Wang Ding J et al. proposed a U-Net network with a residual structure and an attention-gate mechanism (Ding et al., 2019). Rehman et al. proposed integrating a deep learning model with a fully convolutional neural network and a VGG16 backbone had been used to improve detection accuracy (Rehman et al., 2021). The findings demonstrated that the suggested technique beat the U-Net model, obtaining 99% accuracy while being twice as quick. Garg et al. envisioned the CK-SNIFFER object identification system, which uses common sense knowledge to automatically

identify a huge number of errors (Garg et al.,2020).

The purpose of this study is to create an improved classifier of thyroid nodules malignancy based on fused features derived in the first palace from applying VGG16(deep learning features) for each image in the training stage combined with handcraft spatial features derived from FGLCM after segmenting each image in the training stage using VGG19 transfer learning technique based segmentation method namely(VGG-SegNet). After generating the fused features, four types of machine learning have been applied accordingly, Naïve Bayes (NB), Decision Tree (DT), K-Nearest Neighbor (KNN), and Support Vector Machine based Radial Basis Function (SVM-RBF).

2.MATERIAL AND METHOD
2.1 Dataset

It is challenging to collect a significant number of thyroid nodules-based ultrasound images due to time constraints and patient cooperation. As a consequence, we chose to employ a dataset of images of thyroid nodules that were openly available. the collection of digital thyroid pictures. The public can view the Universidad Nacional de Colombia's (TDID) dataset (Pedraza et al., 2015). In a 2015 publication of the TDID dataset had been launched, which contains 400 thyroid ultrasound pictures from 298 different people. Each patient received at least one thyroid ultrasound image. The image has a resolution of 560*360 pixels and a radiologist-written diagnostic description of the supposed thyroid lesions. Based on the ultrasound parameters, each image was graded using the Thyroid Imaging Reporting and Data System (TI-RADS) of the American College of Radiology to assess the probability of thyroid nodule malignancy (Tessler et al.,2018). The TI-RADS score, which aids in categorizing the thyroid nodules into one of the five phases, is used to stage thyroid nodules. TIRADS-5 indicates a significant risk of thyroid cancer, while TIRADS-1 indicates a benign class. 400 fine-needle aspiration histopathology lesions (287 benign and 113 malignant) were collected in JPEG format from a range of ages and sizes for the dataset used in this research.

2.2 Preprocessing of Image Data

Figure 1 depicted the presented system model block diagram which covers all the stages from data collection to classification. The main stages in the proposed system model include data collection, preprocessing, feature extraction, and eventually classification of the training thyroid images to fall into one of two categories namely (Benign and malignant). The following subsections describe each stage briefly.
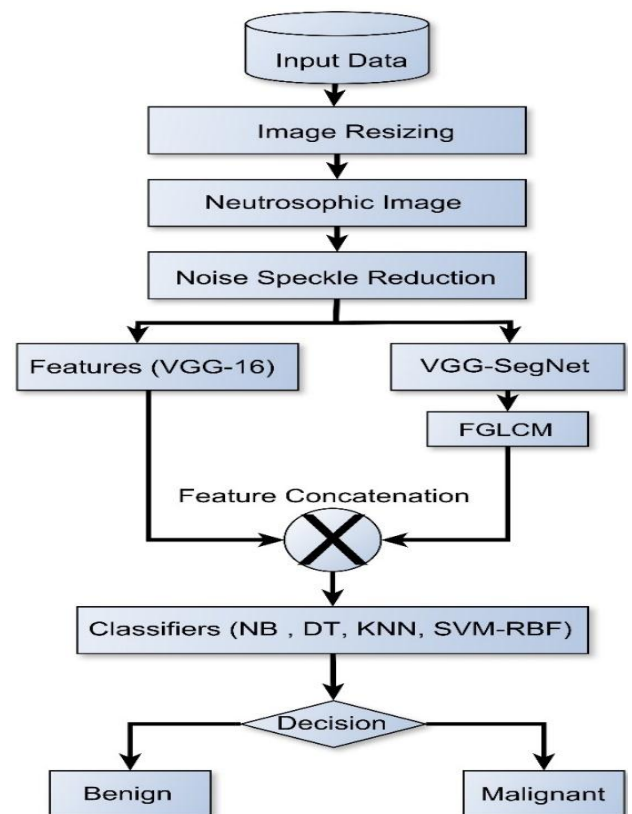
**Figure 1:** The block diagram of the proposed system.

The most important aspect of computer-aided diagnosis (CAD) research is feature extraction, which has a significant contribution to classification methods. The collected images for training are all resized to $224 \times 224 \times 3$ to match the standard input size for the images to the VGG16 and VGG19 techniques which are the core techniques in feature extraction. In this study, the resized images of a thyroid nodule have been enhanced using a joint Neutrosophic enhancement technique (to improve the visual appearance of images to make them more suited for human viewers or machine vision applications) and a Speckle Noise Reduction which is a sort of

filter typically used to remove speckle noise from ultrasound images; it preserves and improves edges (Kim et al., 2022, haji et al., 2019).

2.3 Proposed Features extraction techniques:

The output of the features extraction stage (which starts after the preprocessing process) is a fused features vector, which is generated from features collected from two stages. Thus, in the first stage based on VGG19 a (VGG-SegNet), a segmentation technique is applied to each training image resulting from the preprocessing stage. Figure 2 shows the procedure for generating each segmented nodule image. Model VGG Typically,

the term "VGG-Net" refers to a deep convolutional network for object recognition created and trained by Oxford's famous Visual geometry group (VGG), which displayed excellent results on the ImageNet dataset (Pedraza et al., 2015). Deep learning algorithm VGG-SegNet Segmentation was performed using a VGG-SegNet (encoder-decoder CNN) deep learning model, and the starting weights and layers of the SegNet model was created using pre-trained VGG19 models. The five encoder layers are configured using the layers of VGG19, and the deciphering layers are the same as the encoder layers, as shown in Figure 2.
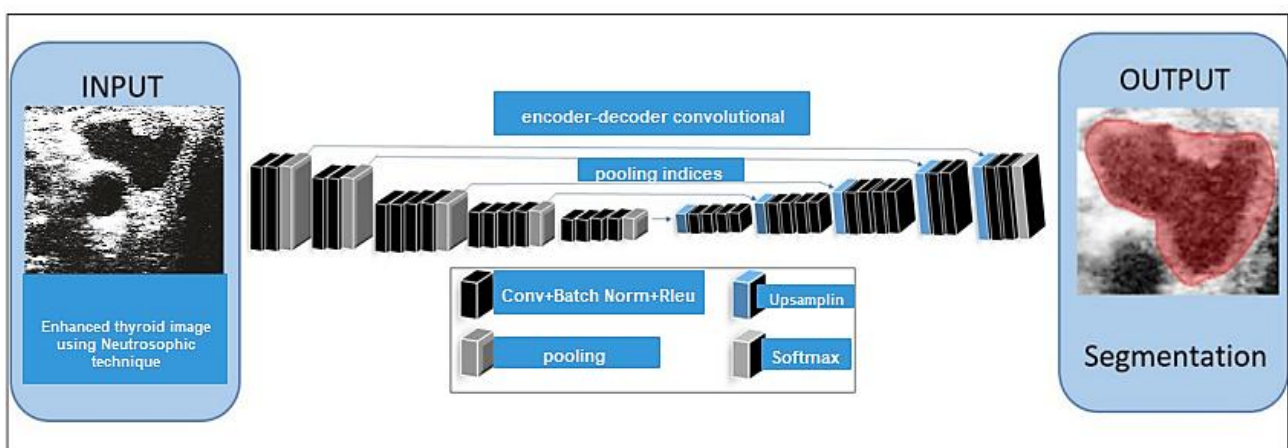
Figure 2: The process of generating a segmented image by VGG-SegNet.

The group norm and ReLU come after each convolutional layer. The initial learning rate is 0.002, the mini-batch size is 2, and Stochastic Gradient Descent with Momentum (SGDM) is used as the optimization method for training, according to the explanation of the training parameters. Only the portion of the segmented image that contains the thyroid nodules will be colored white when the training procedure is complete. In VGG Convolutional layers are stacked on top of one another at rising depths to introduce the VGG network. Max pooling reduces the volume measurement. A softmax classifier is then followed by two completely connected layers with a total of 4,096 nodes each. To minimize the number of parameters in this deep network, VGG employs very small convolution filters (3 ×3), with a convolutional step equal to 1 pixel (Zhang et al., 2015). VGG-Net comes in two models: VGG16 and VGG19. The 144 million parameters

VGG16 consists of 16 convolutional layers with very tiny receptive fields (3x3), 5 max-pooling layers (2x2) for performing spatial pooling, 3 fully connected layers, and a soft-max layer as the final layer (Simonyan et al., 2015).

All hidden levels receive ReLU activation. In the completely connected layers of the model, dropout regularization is also used. More than a million images from the ImageNet database were used to teach VGG16. The size of the input image for the VGG16 model is the matrix of shape 224*224*3 (RGB image) (Mascarenhas and Agarwal., 2015). The total amount of completely connected nodes and deep nodes causes the VGG for VGG16 to be larger than 500 MB. A 16 deep neural network levels make up the VGG16 Neural Network. Less weight is given to the VGG16 network. More than a million images from the ImageNet database were used to teach CNN VGG19 (Russakovsky et al., 2015). A

224*224*3-pixel input picture is used by the VGG19 model (RGB image). Due to the quantity of completely connected nodes and deep nodes, the VGG for VGG19 is larger than 574 MB (Adrian, 2017). 19 levels of deep neural networks make up VGG19. VGG19 network is a more significant model that could classify the images better than VGG16 as well as can improve the computational processing time and learning rate (Alom et al., 2018). Figure 3 depicts the schematic of the VGG16 and VGG19 architecture learned on the ImageNet database.
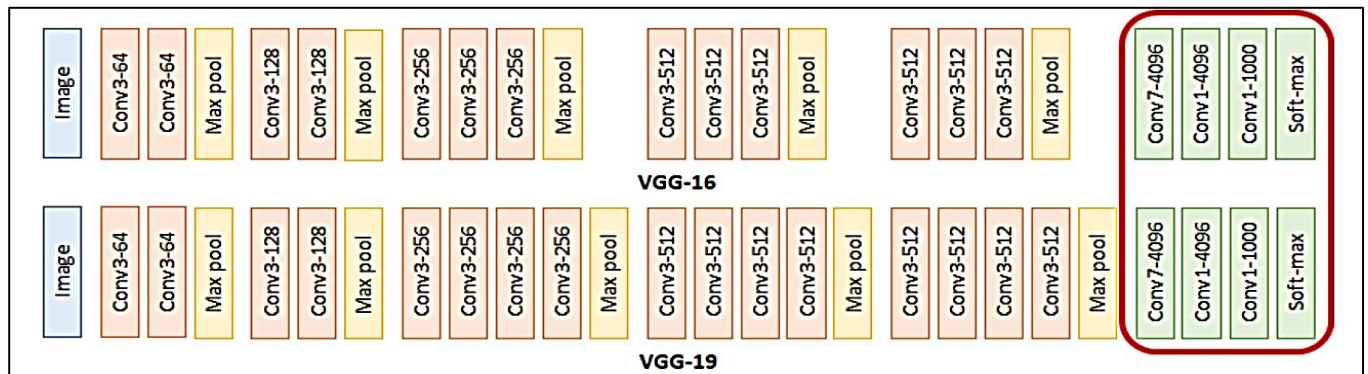
Figure 3: Structure of VGG16 and VGG19 (Shadeed et al., 2020).

In the training stage, the ground truth images from different groups (malignant and benign) are used to evaluate the accuracy of the VGG-SegNet. Thus, images were segmented by making hand-made labels of the thyroid images from different groups and using them later as ground truth images used by transfer learning to perform automatic segmentation. Figure 4 depicts thyroid image samples with associated ground-truth thyroid regions in the TDID dataset. The segmented images were then introduced to the stage of extracting spatial or textural features based on fusing multiple (FGLCM) at four angles $(0^{o}, 45^{o}, 90^{o},$ and $135^{o})$.
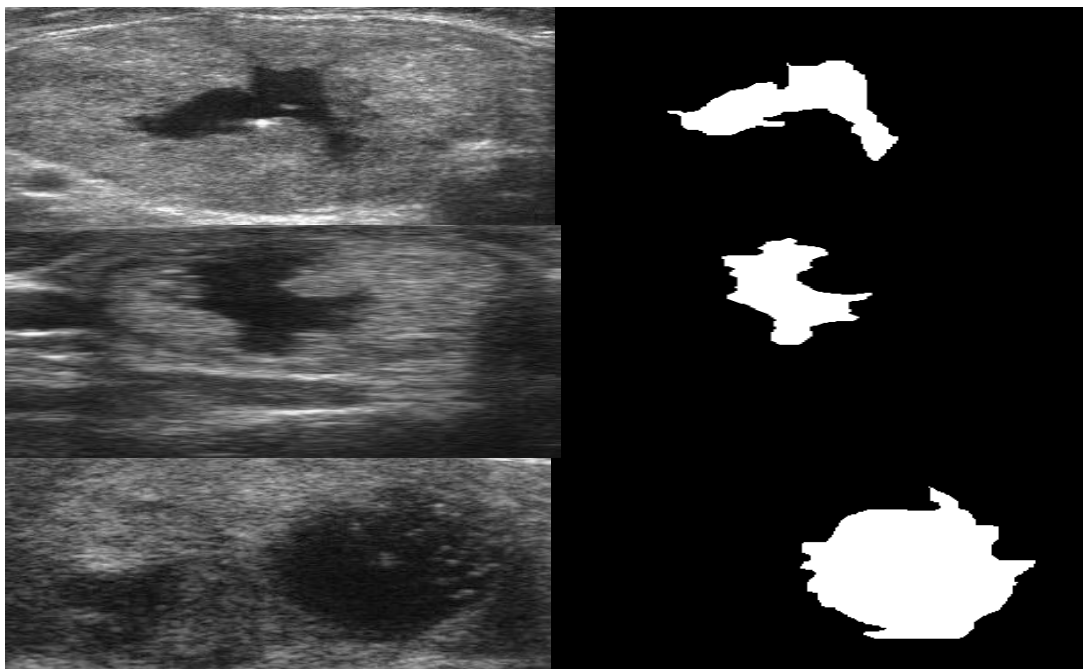
Figure 4: Thyroid image examples in the TDID dataset with corresponding ground-truth thyroid region.

To generate an (FGCM), the Fuzzy C-Mean (FCM) is first applied to each band from the three bands in each input image I. Thus, the FCM can be constructed as: (Zhang et al., 2013):

$$U_{ij} = \cfrac{1}{\sum_{k=1}^{C}\left\{\cfrac{\|X_i - c_j\|}{\|X_i - c_k\|}\right\}^{\frac{2}{m-1}}} \qquad (1)$$

$$c_j = \frac{\sum_{i=1}^{N} U_{ij}^m X_i}{\sum_{i=1}^{N} U_{ij}^m} \qquad (2)$$

where U_{ij} is represented the value of pixel X_j relating to cluster j, c_j represents the center of cluster j, and m is the fuzzifier. Then, each pixel is assigned to the cluster with $m=2$ and $c=8$, which has the highest membership value. Finally, for each angle (θ=0°, 45°, 90°, and 135°), eight FGCM planes are generated, with pairing distance $d=1$. for every pixel i find the pixel j that is d pixels away from i, then determine the designated cluster for pixel j. Suppose i is allocated cluster k and j is assigned cluster l. Initially Set all FGCMs to 0, then after calculating each matrix at each angle based on the equation below:(Zhang et al., 2013):

$$FGCM(n,k,l)=FGCM (n,k,l)+U_{in}+ U_{jn} \qquad (3)$$

where U_{in} and U_{jn} are the pixel membership values for cluster n. Then the five second-order statistics of S FGCM (i,j) (energy, entropy, contrast, homogeneity, and correlation) are calculated to create the 5-dimensional texture vector.

Where $i, j=0,1,\ldots,L-1$ and $1 \le k \le c$.

$$energy_k = \sum_{i,j} S_{FGCM}(k,i,j)^2 \qquad (4)$$

$$entropy_k = -\sum_{i,j} S_{FGCM}(k,i,j)^2 lb\{S_{FGCM}(k,i,j)\} \qquad (5)$$

$$contrast_k = \sum_{i,j} |i-j|^2 S_{FGCM}(k,i,j) \qquad (6)$$

$$homogeneity_k = \sum_{i,j} \frac{S_{FGCM}(k,i,j)}{1+|i-j|} \qquad (7)$$

$$correlation_k = \frac{\sum_{i,j} ij\, S_{FGCM}(k,i,j) - U_i^k U_j^k}{\sigma_i^k \sigma_j^k} \qquad (8)$$

$$U_i^k = \sum_i i \sum_j S_{FGCM}(k,i,j)$$

$$U_j^k = \sum_i j \sum_j S_{FGCM}(k,i,j)$$

$$\sigma_i^k = \sum_i (i - \mu_i^k)^2 S_{FGCM}(k,i,j)$$

$$\sigma_j^k = \sum_j (j - \mu_j^k)^2 S_{FGCM}(k,i,j)$$

It is important to note that several transfer learning approaches, specifically U-Net and VGG16, have been tested for segmented image generation to determine the optimal methodology. pre-trained VGG19 deep-learning classification features are created. A deep learning feature generated by VGG16 of 1*1000 for each image has been generated. The block diagram of this process is described in figure 5 below.
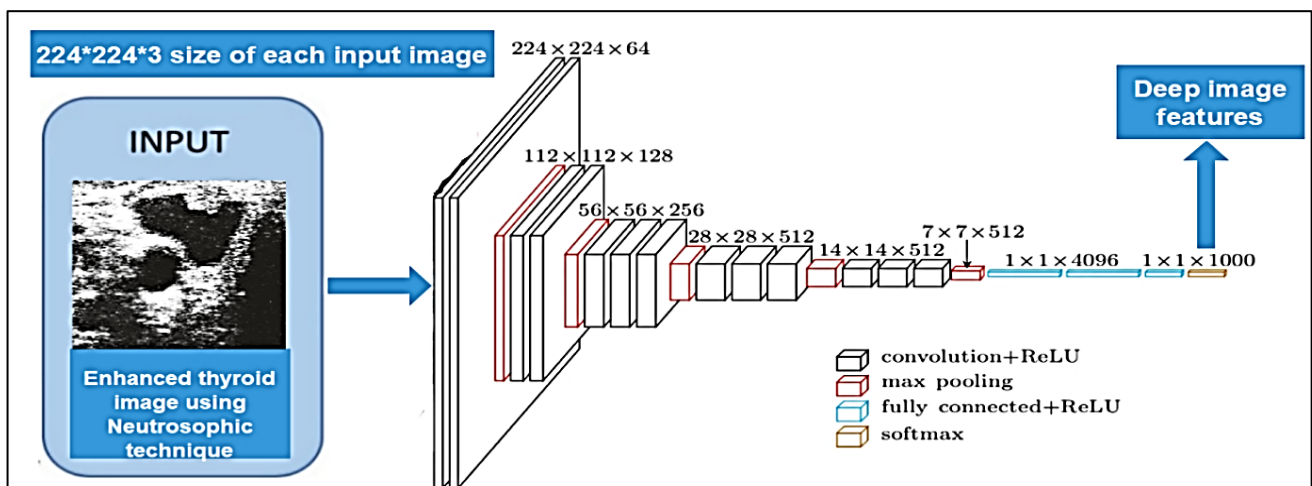

Figure 5: Deep features were extracted for each image.

Eventually, a fused features concatenation between deep learning and textural FGLCM-based VGG-SegNet features are produced. The generated features vector *FV* is made by two folds: *FV1* and *FV2*.where *FV1* are the textural features while *FV2* are the deep learning features as indicated below:

FV1=[Energy, entropy, contrast, homogeneity, correlation]^1 a θ ∈ {0,45,90,135} …[Energy, entropy contrast, homogeneity, correlation]^{301} at θ ∈ {0,45,90,135}. Where (1) represents the first image from the 301 training image (216 benign and 85 malignant). The feature vector FV2 is calculated as:

$$FV2_{VGG16} = VGG16^1_{1*1000} \dots\dots VGG16^{301}_{1*1000} \quad (9)$$

And hence:
$$FV=[FV1|FV2] \quad (10)$$

2.4 Classification stage

The final stage of machine learning classification. To verify the suggested approach, a thorough comparison of several two-class classifiers, including Decision-Tree (DT), K-Nearest Neighbor (KNN), Naive Bayes (NB), and Support Vector Machine-Radial Basis Function (SVM-RBF) are conducted using 10-fold cross-validation (Mohammed et al., 2021) (Haji et al., 2019).

2.1 Evaluation Metrics

The results of segmentation are assessed using parameters such as Accuracy (ACC), Sensitivity (SEN), Specificity (SPE), Precision (PRE), Dice coefficient (DSC), and Negative Predicted Value (NPV). These parameters are explained below (Zhang et al., 2013):

$$Accuracy\ (ACC) = \frac{TP + TN}{TP + TN + FP + FN} \quad (11)$$

$$Sensitivity\ or\ Recall (TPR) = \frac{TP}{TP + FN} \quad (12)$$

$$Specificity(SPE) = \frac{TN}{TN+FP} \quad (13)$$

$$Precision(PRE) = \frac{TP}{TP + FP} \quad (14)$$

$$Dice\ Score\ (DSC) = \frac{2 \times TP}{2 \times TP + FN + FP} \quad (15)$$

$$Negative\ Predictive\ Value(NPV) = \frac{TN}{TN+FN} \quad (16)$$

3.RESULT AND DISCUSSION

Classifying thyroid nodules utilizing various segmentation methods has images from 400 patients, some with benign and others with malignant cases. Table 1 lists the total images evaluated for the analysis.

Table 1: Evaluated thyroid nodule images.

Image Type	Dimensions	Overall Images	Image Training	Imaging Validation
Benign	$224 \times 224 \times 3$	287	216	71
Malignant	$224 \times 224 \times 3$	113	85	28

Primarily, Table 1 contains ultrasound images of thyroid nodules that are resized to 224 * 224 * 3 pixels to create VGG-SegNet-based thyroid nodule images; the test images are then confined to a feature extraction process; a random sample of the Benign and Malignant class images is shown in Figure 6 below. The segmentation technique for US images using encoded and decoded VGG-SegNet and U-Net is illustrated experimentally in Figure 3. From Figure 6 it's

clear that the output segmented images based on VGG19 outperform the other two techniques corresponding to the ground truth images. The accuracy results achieved for these three segmentation techniques corresponding to the ground-truth-related images are reported in Table 2 which proves the superiority of the VGG19-SegNet-based segmentation technique.

Table 2: Performance evaluation Accuracy of different segmentation techniques.

Approach	ACC
VGG19-SegNet	**99.72**
VGG16-SegNet	**98.88**
U-Net	**98.33**

The analysis is continued using the VGG19 technique to derive the integrated DF+FGLCM (1× 1540) features fed to several classifiers, including DT, KNN, NB, and SVM-RBF; the results are shown in Table 3. A 10-fold validation of VGG19 is shown in Figure 4, which also illustrates its performance with SVM-RBF. The result demonstrated in Table 3 confirms the SVM-RBF classifier offers superior outcome contrast to other classifiers. Figure 7 shows the accuracy calculation for the best machine learning technique SVM-RBF with the error rates, it's clear that after 450 epochs the accuracy of the classification reached around 100% (99.25%) with a classification error of almost zero. Table 4 Presented a comparison between the proposed work and other peer literature which demonstrate the superiority of the proposed technique.

Table 3: Comparison of VGG19's disease detection performance using DF+FGLCM and other classifiers.

| Classifier	TP	FN	TN	FP	ACC	PRE	SEN	SPE	NPV	DICE
NB	105	8	282	5	96.75	95.45	92.92	98.26	97.24	94.17
DT	104	9	282	5	96.5	95.41	92.03	98.25	96.91	93.69
KNN	111	2	283	4	98.5	96.52	98.23	98.61	99.29	97.37
SVM-RBF	111	2	286	1	99.25	99.11	98.23	99.65	99.31	98.67

Table 4: Comparison of proposed work with peer literature using the same dataset with different techniques.

Author	Method	Dataset	Accuracy (%)
Rehman et al.	VGG-16 (backbone)	TDID	99
Haji et al.	SSHOS	TDID	96
Nguyen et al.	ResNet + InceptionNet	TDID	92.05
Huitong et al	SGUNET	TDID	93.6
Proposed	VGG-19 features extraction SVM classification segmentation	TDID	99.25
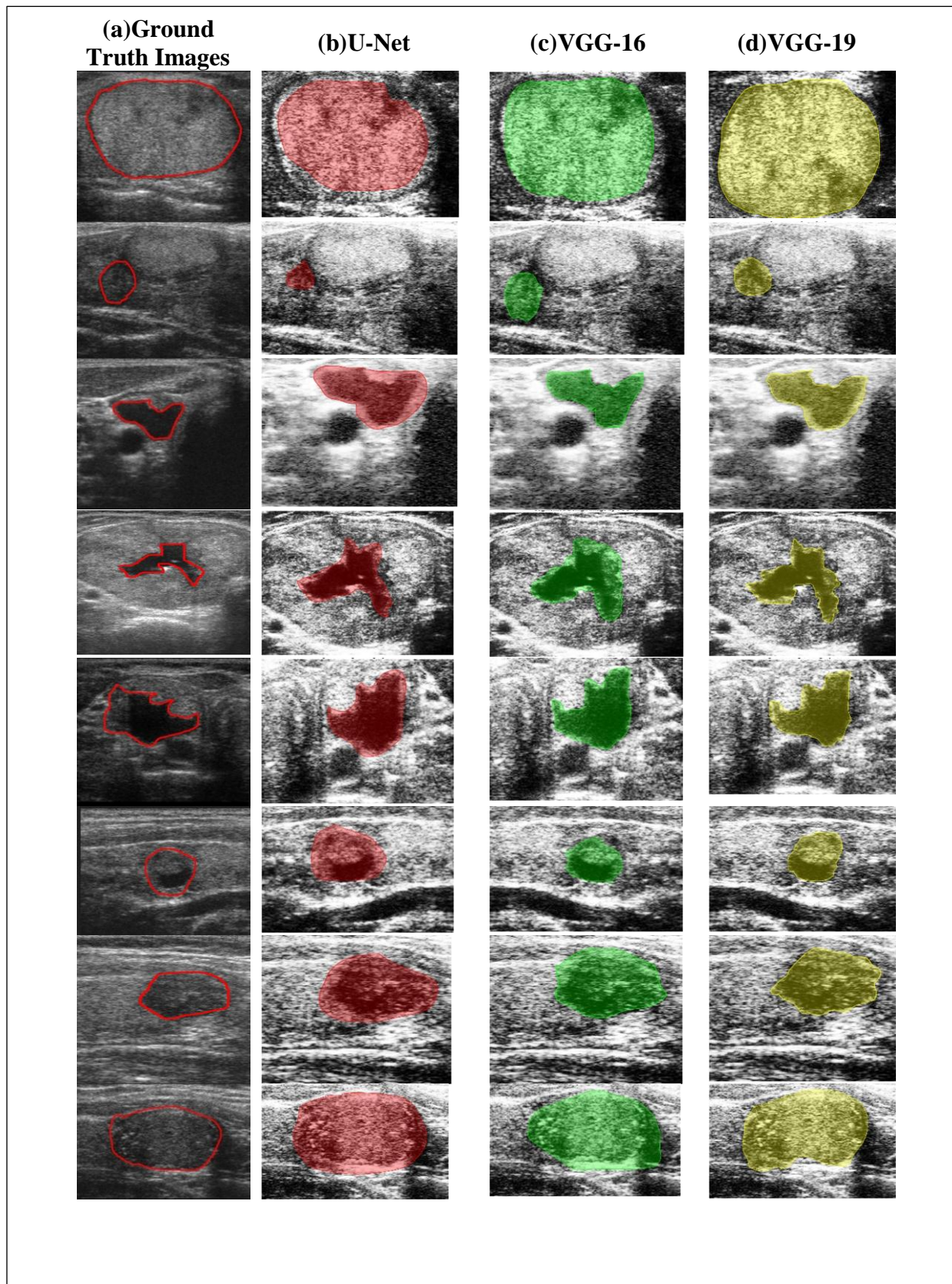
Figure 6. Segmentation of US images using (U-Net, VGG16, and VGG19).
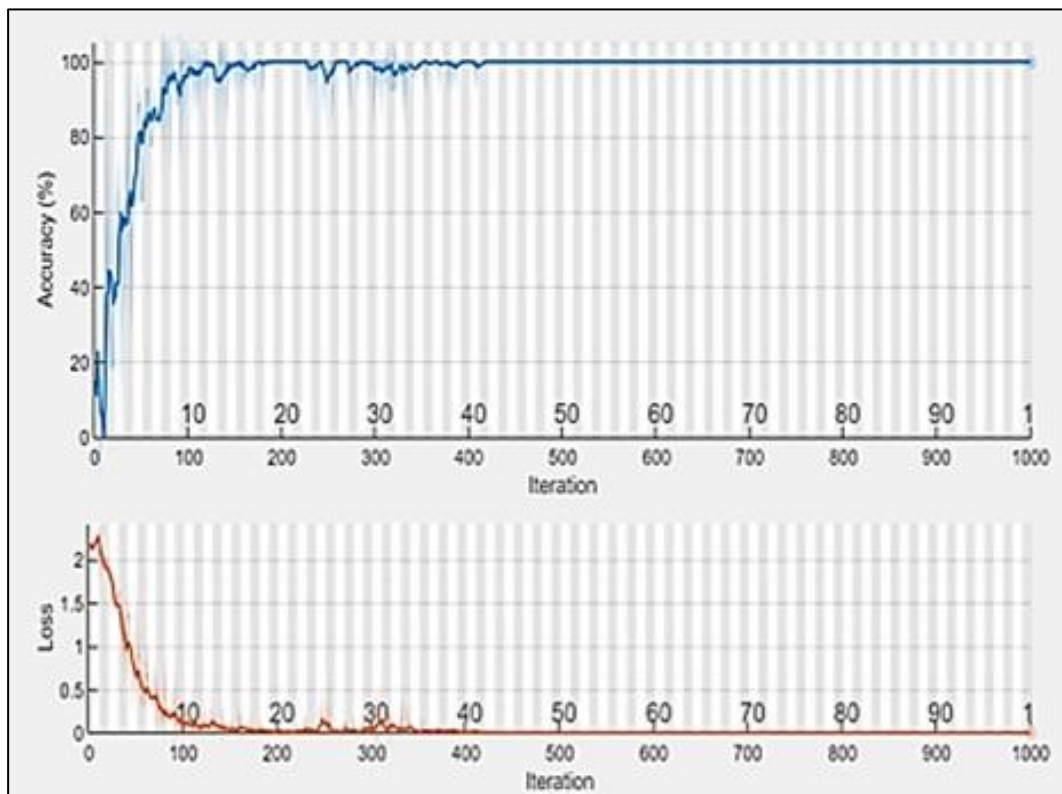
Figure 7. Thyroid nodule ultrasound image classification training progress and loss value using SVM-RBF.

4.CONCLUSION

Thyroid cancer diagnosis relies on the precise ultrasound segmentation of thyroid nodule regions. Sometimes it is not easy to classify benign thyroid cases from malignant, for this objective using a computer-assisted diagnosis system plays an important role in classifying the images. In this study, a new technique has been proposed to discover and optimize pre-trained data based on VGG19-based automated segmentation and classification scheme for analyzing thyroid nodule US images. This scheme is implemented in two phases: first, VGG-SegNet-supported extraction of thyroid nodules from US images is used to extract the FGLCM features in addition to DL-Features (DLF) derived from pre-training the VGG19 Net. Finally, DLF+FGLCM features vector has been constructed. The VGG19-SegNet showed superior results compared to other segmentation techniques (U-Net and VGG16-SegNet) relative to corresponding ground truth images. The SVM-RBF classifier was one of four used on the integrated features (DLF+FGLCM) of US images to improve classification accuracy (99.25%). Experimental results show that the suggested model can be used as a second aim to help radiologists easily segment the thyroid region of interest for sake of classifying benign images from malignant images. The proposed method has the drawback of having a rather high limiting dimension (1×1540) due to the number of concatenated features.

REFERENCES

Acharya, U. R., Chowriappa, P., Fujita, P. et al. 2016 Thyroid lesion classification in 242 patient population using Gabor transform features from high-resolution ultrasound images, Knowledge-Based Systems, 107, pp. 235–245. doi: 10.1016 /j. knosys. 2016.06.010.

Adrian, R. (2017), Image Net: VGGNET, ResNet, Inception, and Xception with Keras. Available at: https://www.pyimagesearch.com/2017/03/20/imagenet-vggnet-resnet-inception-xception-keras/ . (Accessed: 20 March 2020).

Ajilisa, O.A., Jagathy Raj, V.P., and Sabu, M.K. 2022. Segmentation of Thyroid Nodules from Ultrasound Images Using Convolutional Neural Network Architectures. 687 – 705.

Alom, M.Z., Taha, T.M., Yakopcic, C., Westberg, S., Sidike, P., Nasrin, M.S., Van Esesn, B.C.,

Awwal, A.A.S. and Asari, V.K., 2018. The history began from alexnet: A comprehensive survey on deep learning approaches. arXiv preprint arXiv:1803.01164.

Cheng HD, Shan J, Ju W, Guo Y, Zhang L. 2010. Automated breast cancer detection and classification using ultrasound images: A survey. Pattern Recognit. 43(1):299-317. doi:10.1016/j.patcog.2009.05.012

Ding, J., Z. Huang, M. Shi and C. Ning. 2019. Automatic Thyroid Ultrasound Image Segmentation Based on U-shaped Network. 12th International Congress on Image and Signal Processing, BioMedical Engineering and Informatics (CISP-BMEI).

Garg A, Tandon N, Varde A. 2020. I am guessing you can't recognize this: generating adversarial images for object detection using spatial commonsense (student abstract). Proc AAAI Conf Artif Intell 34(10):13789–13790. https://doi.org/10.1609/aaai.v34i10.7166.

Haji, S. O., and R. Z. Yousif. 2019. A Novel Neutrosophic Method for Automatic Seed Point Selection in Thyroid Nodule Images. BioMed Research International. 1, 1-14.

Haji, S.O. and Yousif, R.Z., 2019. A novel run-length based wavelet features for screening thyroid nodule malignancy. Brazilian Archives of Biology and Technology, 62.

Karthikeyan D, Varde AS, Wang W. 2020).Transfer learning for decision support in Covid-19 detection from a few images in big data. IEEE Int Conf Big Data (big Data)4873–4881. https://doi.org/10.1109/BigData50022.2020.9377886.

Kataoka H, Iwata K, Satoh Y. 2015. Feature evaluation of deep convolutional neural networks for object recognition and detection. https://arxiv.org/abs/1509.07627

Kim, K.; Chon, N.; Jeong, H.-W.; Lee, Y. 2022. Improvement of Ultrasound Image Quality Using Non-Local Means Noise-Reduction Approach for Precise Quality Control and Accurate Diagnosis of Thyroid Nodules. Int. J. Environ. Res. Public Health, 19, 13743. https://doi.org/10.3390/ijerph192113743

Koundal, D., Gupta, S. and Singh, S. 2018. Biomedical Signal Processing and Control Computer-aided thyroid nodule detection system using medical ultrasound images', Biomedical Signal Processing and Control. Elsevier Ltd, 40, pp. 117–130. doi: 10.1016/j.bspc.2017.08.025.

Li, X., Zhang, S., Zhang, Q., Wei, X., Pan, Y., Zhao, J., Xin, X., Qin, C., Wang, X., Li, J.; et al.2019. Diagnosis of thyroid cancer using deep convolutional neural network models applied to sonographic images: A retrospective, multicohort, diagnostic study. Lancet Oncol. 20, 193–201. [CrossRef]

Ma, J. L., F. Wu, T. A. Jiang, Q. Y. Zhao and D. X. Kong. 2017. Ultrasound image-based thyroid nodule automatic segmentation using convolutional neural networks. International Journal of Computer Assisted Radiology and Surgery 12(11):1895-1910, https://doi.org/10.1007/s11548-017-1649-7

Mascarenhas, S. and Agarwal, M., 2021, November. A comparison between VGG16, VGG19 and ResNet50 architecture frameworks for Image Classification. In 2021 International Conference on Disruptive Technologies for Multi-Disciplinary Research and Applications 1(1), pp. 96-99.

Mohammed, B.N., Al-Mukhtar, F.H., Yousif, R.Z. and Almashhadani, Y.S., 2021. Automatic Classification of Covid-19 Chest X-Ray Images Using Local Binary Pattern and Binary Particle Swarm Optimization for Feature Selection. Cihan University-Erbil Scientific Journal, 5(2), pp.46-51.

Nguyen, D.T., Kang, J.K., Pham, T.D., Batchuluun, G., Park, K.R.2022. Ultrasound Image-Based Diagnosis of Malignant Thyroid Nodule Using Artificial Intelligence. Sensors, 20, 1822. [CrossRef]

Pedraza, L., Vargas, C., Narváez, F., Durán, O., Muñoz, E., Romero, E. 2015. An open-access thyroid ultrasound image database. In Proceedings of the 10th International Symposium on Medical Information Processing and Analysis, Cartagena de Indias, Colombia, 28 January; Volume 9287, pp. 1–6.

Prochazka, A., Gulati, S., Holinka, S., Smutek, D. 2019. Classification of Thyroid Nodules in Ultrasound Images Using DirectionIndependent Features Extracted by Two-Threshold Binary Decomposition. Technol. Cancer Res. Treat.18, 1533033819830748. [CrossRef] [PubMed].

Rajinikanth, V., Joseph Raj, A.N., Thanaraj, K.P., Naik, G.R. 2020. A Customized VGG19 Network with Concatenation of Deep and Handcrafted Features for Brain Tumor Detection. Appl. Sci. 10, 3429. [CrossRef]

Rehman, H.A.U.; Lin, C.-Y.; Su, S.-F. 2021. Deep Learning Based Fast Screening Approach on Ultrasound Images for Thyroid Nodules Diagnosis. Diagnostics, 11, 2209. https://doi.org/10.3390/.

Russakovsky, O., Deng, J., Su, H., Krause, J., Satheesh, S., Ma, S., Huang, Z., Karpathy, A., Khosla, A., Bernstein, M. and Berg, A.C., 2015. Imagenet large scale visual recognition challenge. International journal of computer vision, 115, pp.211-252.

Simonyan, K., Zisserman, A. 2014. Very Deep Convolutional Networks for Large-Scale Image Recognition, in: ICLR 2015. Presented at the 3rd International Conference on Learning Representations, San Diego, CA.

Shadeed, G.A., Tawfeeq, M.A. and Mahmoud, S.M., 2020, June. Automatic Medical Images Segmentation Based on Deep Learning Networks. In IOP Conference Series: Materials Science and Engineering 870 (1), pp. 012117 IOP Publishing.

Sharifi, Y., Bakhshali, M.A., Dehghani, T., DanaiAshgzari, M.; Sargolzaei, M.; Eslami, S. 2021. Deep learning on ultrasound images of thyroid nodules. Biocybern. Biomed. Eng. 41, 636–655. [CrossRef]

Tessler,F.N.; Middleton, W.D; Grant, EG. 2018. Thyroid Imaging reporting and Data System (TI-RADS): A User's Guide. Radiology, 287,29-36.[CrossRef][PubMed].

Vasile, C., Udris,toiu, A., Ghenea, A., Popescu, M., Gheonea, C., Niculescu, C., Ungureanu, A., Udris,toiu, S, ., Droca¸s, A., Gruionu, L., et al. 2021. Intelligent Diagnosis of Thyroid Ultrasound Imaging Using an Ensemble of Deep Learning Methods. Medicine, 57, 395. [CrossRef].

Wang Xin and Xu Wenjie. 2016. Research on Ultrasound Image Segmentation Algorithm of Thyroid Nodules. Television Technology 40(08): 26-30+56,
https://doi.org/10.16280/j.videoe.2016.08.005

Yang J, Shi X, Wang B, Qiu W, Tian G, Wang X, Wang P and Yang J. 2022. Ultrasound Image Classification of Thyroid Nodules Based on Deep Learning. Front. Oncol. 12:905955. doi: 10.3389/fonc.2022.905955

Ying, X., Z. H. Yu, R. G. Yu, X. W. Li, M. Yu, M. K. Zhao and K. Liu. 2018. Thyroid Nodule Segmentation in Ultrasound Images Based on Cascaded Convolutional Neural Network. Neural Information Processing (Iconip 2018), Pt Vi 11306: 373-384, https://doi.org/10.1007/978-3-030-04224-0_32.

Zhang,Feng, and Bao-jiang ZONG. 2016. Image Retrieval Based on Fused CNN Features."DEStech Transactions on Computer Science and Engineering aics.

Zhang S, She L. H., Lu L., Zhong H. 2013. A Modified Fuzzy C-Means for Bias Field Estimation and Segmentation of Brain MR Image, Proceedings of the 25th Chinese Control and Decision Conference, 2080-2085.